Clays and Clay Minerals, Vol. 59, No. 5, 507–517, 2011.

MODIFICATION OF MONTMORILLONITE WITH POLY(OXYPROPYLENE) AMINE HYDROCHLORIDES: BASAL SPACING, AMOUNT INTERCALATED, AND THERMAL STABILITY

YAQING WANG, XIAOQUN WANG*, YIFENG DUAN, YUZHONG LIU, AND SHANYI DU

School of Material Science and Engineering, Beihang University, Beijing 100191, China

Abstract—Few studies have explored the change in thermal stability of poly(oxypropylene) (POP) ammonium ions after intercalation, even though several studies have focused on the modification of montmorillonite (Mt) with POP amine hydrochloride. The purpose of the present study was to understand the effect of chain length of POP amine hydrochlorides on the basal spacing of modified Mt, and the amount and thermal stability of the ammonium ions intercalated. The relations between basal spacing, organic fraction, and thermal stability of the ammonium ions intercalated were also explored. Series of modified Mt were prepared *via* ion-exchange between Na-montmorillonite (Na^+-Mt) and POP diammonium ions or POP triammonium ions with different chain lengths, and were then characterized by Fourier-transform infrared spectroscopy, X-ray diffraction, and simultaneous differential scanning calorimetry-thermogravimetric analysis. The results revealed that the basal spacing of modified Mt increased with the hydrophobic chain length of the POP ammonium ions. The amount of triammonium ions intercalated was close to the theoretical amount, while the organic fraction of modified Mt was directly proportional to the basal spacing of modified Mt. The intercalated ammonium ions were, therefore, contained within the interlayer space of Mt. After intercalation, the thermal stability of the POP ammonium ions with various chain lengths was reduced; *i.e.* T_{onset} was reduced by 7−60ºC for short-chain POP ammonium ions (D400 and T403) and by 177−192ºC for long-chain ions (D2000, D4000, T3000, and T5000).

Key Words—Chain Length, Montmorillonite, POP Ammonium Ion, Thermal Stability.

INTRODUCTION

Smectite is an abundant, cheap, and largely non-toxic inorganic, layered material which has large cation exchange capacity, swelling capacity, surface area, and adsorption capacity; it is used widely in a range of applications, including as a catalyst, an absorbent, in biomaterial encapsulation, in modified electrodes, in self-assembling substrates, and in nanocomposites (Jaber and Lambert, 2010; Laza *et al.*, 2007; Lebaron *et al.*, 1999; Xi *et al.*, 2004; Yadav and Rai, 2006; Lin *et al.*, 2008; Hrachová *et al.*, 2009; Šucha *et al.*, 2009; Guegan *et al.*, 2009; Monvisade and Siriphannon, 2009). Among expanding clays, the most commonly used dioctahedral smectite is montmorillonite (Mt) which has excellent swelling ability, and can be intercalated easily (Xi *et al.*, 2005). Recent developments in the use of Mt have mainly been in the area of environmental remediation, such as treatment of oil spills and waste water, and in the area of clay/polymer nanocomposites (CPN) with improved properties, for gas barriers, solvent resistance, thermal stability, and mechanical properties (Lebaron *et al.*, 1999; Pinnavaia and Beall, 2000; Alexandre and Dubois, 2000; Chen and Yang, 2002; Becker *et al.*, 2002; Kong and Park, 2003; Guan *et al.*, 2005; Hrachová *et al.*, 2009).

Changes in the properties of CPN are known to be affected mainly by the dispersion state of Mt in the polymer matrix (Zhao and Samulski, 2006; Gu *et al.*, 2010). To achieve optimal improvement, the clay layers should be dispersed as single platelets throughout the polymer matrix, a process known as exfoliation (Bergaya *et al.*, 2011; Esfandiari *et al.*, 2008). Due to the small basal spacing, hydrophilicity, and lack of affinity for the hydrophobic organic compounds, however, pristine Mt interlayers cannot be penetrated by polymer, and so cannot be exfoliated in the polymer matrix. A similar problem exists in the interaction between pristine Mt and non-ionic organic contaminants (NOCs) when Mt is used as a sorbent in environmental remediation. The Mt must, therefore, be modified with organic chemicals in order to expand the Mt interlayer space and improve its compatibility with polymers or NOCs, so that the Mt can be used as a filler in CPN or as a sorbent in environmental remediation.

Among various organic chemicals used to modify Mt, the most common surfactants are alkylammonium salts, *e.g.* octadecylammonium bromide and octadecyl triethylammonium bromide. The interlayer expansion is limited, however (Lagaly and Weiss, 1969; Lagaly, 1981, 1986; Bergaya and Lagaly, 2001; Bergaya *et al.*, 2006; Paiva *et al.*, 2008).

* E-mail address of corresponding author:
wangxiaoqun@buaa.edu.cn
DOI: 10.1346/CCMN.2011.0590508

https://doi.org/10.1346/CCMN.2011.0590508 Published online by Cambridge University Press

To further expand the basal spacing in Mt, studies in the past decade (Lin and Chen, 2004; Lin *et al.*, 2001; Chou *et al.*, 2003; Hsu *et al.*, 2010) have attempted to intercalate long-chain POP ammonium ions into Mt, and modified Mt with basal spacings of up to 9.2 nm have been obtained. On the basis of the significantly expanded interlayer space, the exfoliated nanocomposites can be prepared readily, including epoxy/Mt nanocomposites, polyurethane/Mt nanocomposites, and polystyrene/Mt nanocomposites (Lin *et al.*, 2001, 2003, 2004, 2007; Salahuddin, 2004; Salahuddin *et al.*, 2010; Yoon *et al.*, 2007).

Besides its use in exfoliated CPN, Mt modified with POP ammonium ions can also be used as an excellent absorbent of oil because, after modification, the enlarged basal spacing and organophilic interlayer enhances the ability of modified Mt to adsorb NOCs (Mortland *et al.*, 1986; Boyd *et al.*, 1988; Jaynes and Boyd, 1991; Guegan *et al.*, 2009; Hsu *et al.*, 2010). The modified Mt can also be further intercalated by other components, *e.g.* magnetic Fe oxide nanoparticles (FeNPs) can be embedded into the modified Mt by POP ammonium ions in order to prepare a novel magnetic nanohybrid. A nanohybrid prepared for oil adsorption with the ability to be attracted by an applied magnetic field, is more useful than conventional absorbents for absorbing and then collecting waste products (Gupta and Suhas, 2009; Hsu *et al.*, 2010).

A number of studies have been carried out on the basal spacing and the organic fraction of Mt modified with a series of POP ammonium ions (*e.g.* Lin *et al.*, 2003, 2004). In contrast, few studies have explored the change in thermal stability of POP ammonium ions after intercalation. The purpose of the present study was to understand the effect of chain length of POP amine hydrochlorides on basal spacing of modified Mt, the amount intercalated, and the thermal stability of the ammonium ions intercalated. The relations between basal spacing, organic fraction, and the thermal stability of the ammonium ions in Mt were also explored through characterization of Mt modified with POP diammonium ions or triammonium ions using X-ray diffraction (XRD), simultaneous differential scanning calorimetry-thermogravimetric analysis (DSC-TGA), and Fourier-transform infrared (FTIR) spectroscopy. The results will be useful in the application of modified Mt in the areas of pollution prevention, environmental remediation, and clay/polymer nanocomposites.

MATERIALS AND METHODS

Materials

Na-montmorillonite (Na^+-Mt) was purchased from Zhejiang Fenghong Clay Chemicals Co., Ltd. (Huzhou, Zhejiang Province, China); the cation exchange capacity (CEC) was 100 meq/100 g. Six POP amines were obtained from Huntsman Corporation (The Woodlands, Texas, USA), including three POP diamines (Jeffamine®D400, D2000, D4000), with average molecular weights of 430, 2000, and 4000 a.m.u., respectively, and three primary polyethertriamines (Jeffamine®T403, T3000, and T5000), with average molecular weights of 440, 3000, and 5000 a.m.u., respectively. The chemical structures of these compounds are presented (Figure 1).

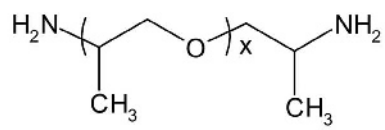

JEFFAMINE	Degree of polymerization	M_w
D400	6.1	430
D2000	33	2000
D4000	68	4000

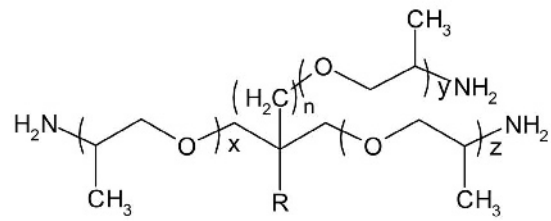

JEFFAMINE	R	*n*	Degree of polymerization	M_w
T403	C_2H_5	1	5-6	440
T3000	H	0	50	3000
T5000	H	0	85	5000

Figure 1. Chemical structures of POP amines.

https://doi.org/10.1346/CCMN.2011.0590508 Published online by Cambridge University Press

Preparation of modified montmorillonite

Preparation of POP amine hydrochloride. Jeffamine®D400 (9 mmol, 3.87 g) and aqueous hydrochloric acid (37 wt.%, 18 mmol, 1.776 g) were dispersed in 484 mL of deionized water for 3 h while cooling in iced water. The other five POP amines underwent the same procedure, where the molar ratio of the amino group to the hydrogen ion was 1:1. Where the POP amine was found not to dissolve completely in deionized water, a water/acetone mixture (molar ratio of water/acetone = 1:3) was used instead of pure water.

Modification of Mt. Na^+-Mt (4 g) was added to a D400 hydrochloride/water solution and stirred steadily using a magnetic stirrer (200–250 r/min) under different reaction conditions, illustrated below (Table 1). The modified Mt was then centrifuged (1500 × g for 30 min). A sample of the modified Mt was examined by XRD immediately after centrifugation; the others were washed three times with deionized water, dried under vacuum at 70ºC for 2 days, and stored under drying conditions for analysis by FTIR and DSC-TGA. The Mt modified with POP amine hydrochloride was prepared using the same procedure, to yield a molar ratio of POP ammonium ion to Na^+ of 2.25:1.

The modified Mts were labeled according to the trademark name of the POP amines as given below: D400-Mt, D2000-Mt, D4000-Mt, T403-Mt, T3000-Mt, and T5000-Mt.

Characterization methods

The modified Mt was analyzed by XRD and, after drying under vacuum at 70ºC for 2 days, by FTIR and differential scanning calorimetry-thermogravimetric analysis (DSC-TGA).

The XRD patterns of Na^+-Mt and modified Mt were collected using a Rigaku (D/Max2200) X-ray diffractometer from the Rigaku Corporation (Tokyo, Japan) with Ni-filtered CuKα radiation (40 kV, 40 mA) from 3 to 20º2θ at a speed of 2º2θ min^{-1}. The basal spacings were calculated according to Bragg's law.

The DSC-TGA analysis of Na^+-Mt and modified Mt was carried out using a thermo analyzer STA 449 C from the Netzsch Group (Selb, Bavaria, Germany). Samples of ~6.5 mg were heated from room temperature to 900ºC at a heating rate of 10ºC/min in a high-purity flowing N_2 atmosphere (60 cm^3/min).

The FTIR spectra of Na^+-Mt, modified Mt, POP amines, and their hydrochlorides were recorded using a Nicolet AVATAR 360 FTIR spectrometer (Nicolet Instruments Inc., Madison, Wisconsin, USA). Sixteen scans were collected for each measurement over the spectral range 400–4000 cm^{-1} with a resolution of 4 cm^{-1}.

Table 1. Illustration of the reaction conditions for preparation of modified Mt.

Reaction temperature (ºC)	Reaction time (h) 2	4	6	8	10	12
10	–	–	–	–	–	+
20	–	–	–	–	–	+
45	–	–	–	–	–	+
70	+	+	+	+	+	+

+ adopted condition; – unadopted condition

RESULTS AND DISCUSSION

In order to identify the optimal reaction conditions, Mt was modified with a series of POP amine hydrochlorides at different reaction temperatures (10, 20, 45, and 70ºC) for 12 h. The basal spacing of the modified Mt (Figure 2) did not change significantly with increased temperature. On the basis of that result, 70ºC was chosen as the temperature for the ion-exchange reaction. The reaction at 70ºC reached equilibrium within 2 h of contact time, and a reaction time of 6 h was generally used in the following experiments.

The FTIR analysis was performed on the POP amines, POP amine hydrochlorides, and modified Mts to confirm the ion exchange between Na^+ and $-NH_3^+$ (Figure 3). Vibrations of $-NH_3^+$ at 3445 cm^{-1} (stretching vibration), 2023 cm^{-1}, and 1624 cm^{-1} (bending vibrations) appeared in the FTIR spectra of D4000 hydrochloride (Figure 3a), indicating that the amino groups had been protonated by the ion exchange with Na^+. The peaks at 2972 cm^{-1} ($-CH_2-$ asymmetric stretching vibration), 2866 cm^{-1} ($-CH_2-$ symmetric stretching vibration), 1454 cm^{-1} ($-CH_2-$ asymmetric bending vibration), 1379 cm^{-1} ($-CH_3$ symmetric bending vibration), and 2069 cm^{-1} ($-NH_3^+$ vibration), were observed in the FTIR spectrum of D4000-Mt but were absent from the spectrum of Na^+-Mt. The appearance of the $-CH_2-$ and the $-NH_3^+$ vibrations provided strong evidence of the interaction between organic species and the Mt interlayer surface, which occurs through the ammonium functional group. A similar

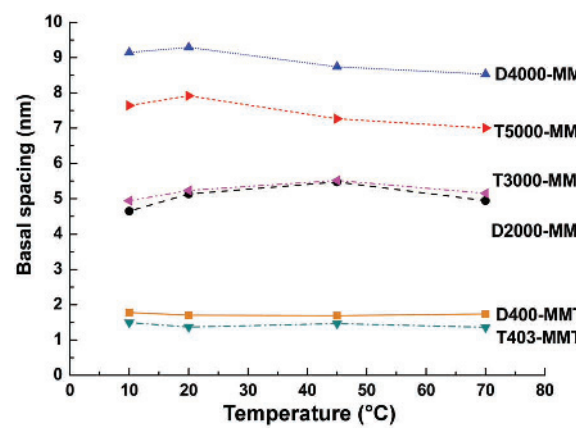

Figure 2. Changes in basal spacing of modified Mt treated for 12 h as function of reaction temperature.

https://doi.org/10.1346/CCMN.2011.0590508 Published online by Cambridge University Press

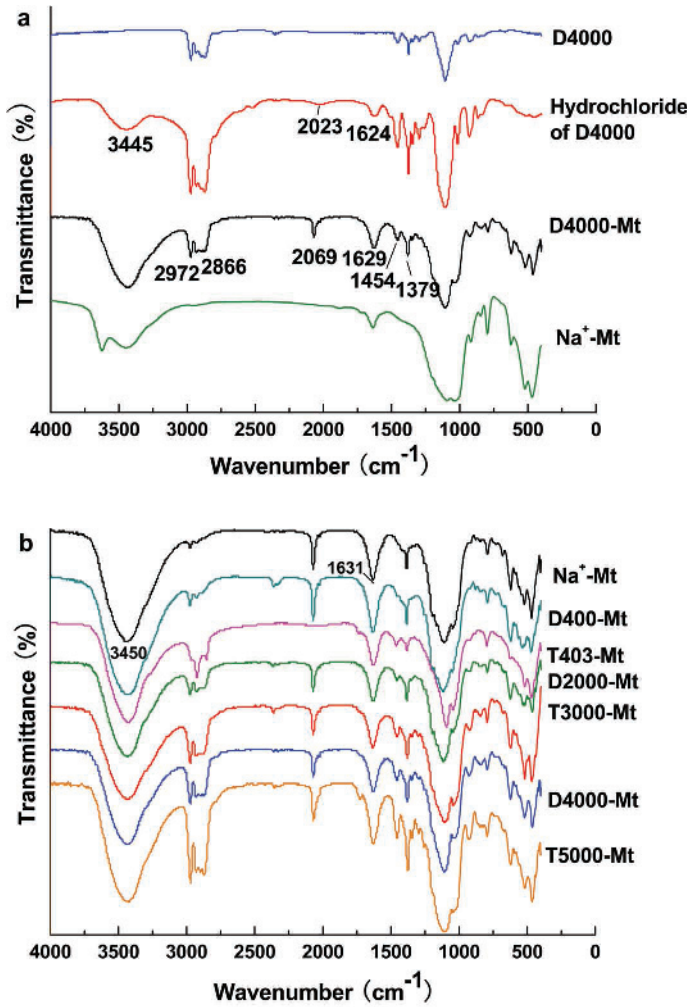

Figure 3. (a) FTIR spectra of Na^+-Mt, D4000-Mt, D4000 hydrochloride, and D4000; (b) FTIR spectra of Na^+-Mt and the modified Mt.

behavior was observed for the other five modified Mts (Figure 3b). The FTIR spectra of both Na^+-Mt and modified Mt (Figure 3b) revealed a strong band at 3450 cm^{-1} and a sharp band at 1631 cm^{-1}, due to H–O–H vibrations of the adsorbed water (Hrachová *et al.*, 2009). The presence of the band relative to the H–O–H vibrations emphasized that, although modified Mts were conventionally considered hydrophobic, water adsorption still occurred. The result was confirmed by DSC-TGA (Figure 8). Similar results were observed for the intercalation of triethylene glycol monodecyl ether ($C_{10}E_3$) non-ionic surfactant into Ca-montmorillonite (Guegan *et al.*, 2009) and in the intercalation of dodecyltrimethylammonium (DDTMA) bromide into rectorite (Li and Jiang, 2009).

Effect of chain length on basal spacing

The XRD patterns of Na^+-Mt and six modified Mts (Figure 4) revealed that both D400-Mt and T403-Mt showed a single diffraction peak (at 5.02 and 5.74º2θ) indicating that the basal spacings were 1.76 nm and 1.54 nm, respectively. When using long-chain POP ammonium ions (D2000, D4000, T3000, and T5000) as intercalating agents, the modified Mt exhibited a series of Bragg peaks in a pattern from $n = 2$ to 5, indicative of a more ordered organic interlayer structure compared to the patterns of Na^+-Mt, D400-Mt, and T403-Mt. According to the formula for calculating the interplanar spacing for any crystal system (equation 1):

$$d_{hkl} = (h2a^{*2} + k^2b^{*2} + l^2c^{*2} + 2hka^*b^*\cos\gamma^* + 2hla^*c^*\cos\beta^* + 2hkb^*c^*\cos\alpha^*)^{-1/2} \quad (1)$$

where d_{hkl} is (h,k,l) interplanar spacing, a^*, b^*, c^*, α^*, β^*, and γ^* are the lattice constants of reciprocal lattice, and h, k, and l are Miller indices (Wang and Zang, 1991). Thus, equation 2 can be deduced,

$$d_{nh,nk,nl} = 1/n(d_{hkl}) \quad (2)$$

where $d_{nh,nk,nl}$ is (nh,nk,nl) interplanar spacing, and d_{hkl} is (h,k,l) interplanar spacing (Wang and Zang, 1991).

https://doi.org/10.1346/CCMN.2011.0590508 Published online by Cambridge University Press

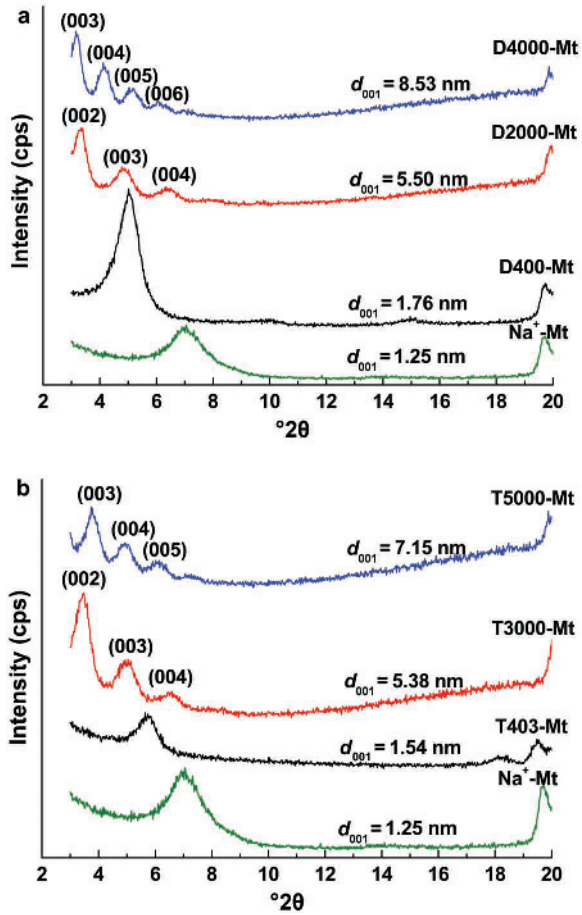

Figure 4. XRD patterns of Na^+-Mt and organically modified Mt: (a) Mt modified with POP diammonium ions; (b) Mt modified with POP triammonium POP ions.

Thus, equation 3 is valid

$$d_{001}:d_{002}:d_{003}:d_{004}:d_{005} = 5:2.5:1.67:1.25:1 \quad (3)$$

The d values of the existing diffraction peaks of the Mt modified with the long-chain POP ammonium ions were in accord with the equations. The first peak in the XRD patterns was, therefore, the (002) diffraction peak (for D2000-Mt and T3000-Mt) or (003) diffraction peak (for D4000-Mt and T5000-Mt). The (001) diffraction peak was at <3°2θ, and thus it was invisible in the XRD patterns. The d_{001} was calculated on the basis of the equation 3.

To demonstrate that this method of calculating d_{001} is valid, a Mt modified with a long-chain POP ammonium ion, T5000-Mt, was tested using both small-angle X-ray diffraction (SAXRD), from 0.6 to 20°2θ at a speed of 2°2θ min^{-1}, and conventional XRD from 3 to 20°2θ at a speed of 2°2θ min^{-1}. The two curves (Figure 5) revealed that the d_{001} value from the calculation method using XRD data was quite close to the d_{001} shown in the SAXRD pattern. The peaks in the XRD patterns also appeared to correspond to analogous peaks in the

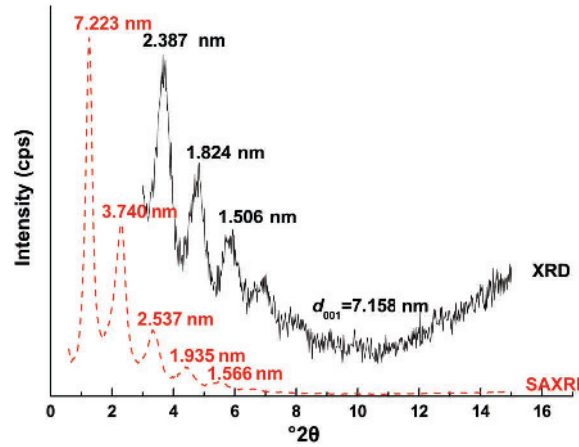

Figure 5. XRD and SAXRD patterns of T5000-Mt.

SAXRD pattern. Hence, the method of calculation was correct.

According to equation 3, the basal spacings of D2000-Mt, D4000-Mt, T3000-Mt, and T5000-Mt were 5.50, 8.53, 5.38, and 7.15 nm, respectively (Figure 4a,b). For all six POP ammine hydrochlorides, the basal spacings of the modified Mt were much larger than that of Na^+-Mt (1.25 nm), indicating that the organic ammonium ions had intercalated into the interlayers of Mt. Clearly, the basal spacings of modified Mts increased with increasing chain length for both diammonium ions or triammonium ions.

To investigate the effect of chain length on the basal spacing of modified Mt, the theoretical length of the fully stretched POP amine backbone was calculated based on bond lengths (0.154 nm for C−C and 0.143 nm for C−O) and bond angles (109.6° for C−C and 112° for C−O) (Lin *et al.*, 2001), and the incremental basal spacing (Δd) was calculated using the formula:

$$\Delta d = d_{(\text{modified Mt})} - d_{(\text{layer unit})} \quad (4)$$

where $d_{(\text{modified Mt})}$ is the basal spacing of the modified Mt, and $d_{(\text{layer unit})}$ is the layer unit basal distance, 0.93 nm (Bergaya *et al.*, 2006; Salahuddin, 2004).

The basal spacing of D400-Mt (1.76 nm) and T403-Mt (1.54 nm) was greater than the theoretical lengths of the D400 (1.4 nm) and T403 ions (1.4 nm) (Table 2). The D400 and T403 ions (short-chain) tended to lie flat on the silicate surface because a tilting or lateral bilayer arrangement was energetically unstable due to the electrical repulsion between unreacted ammonium ions. Moreover, the basal spacing increment of D400-Mt (0.83 nm) was more than twice as long as the theoretical thickness of the D400 ion chain (at least 0.24 nm), which was evaluated assuming the chain was fully stretched. Considering that a flat three-layer arrangement was also energetically unstable, D400 ion may lie as bilayers, whereas the T403 ion may lie as a monolayer (Figure 6a,b), because the incremental basal

https://doi.org/10.1346/CCMN.2011.0590508 Published online by Cambridge University Press

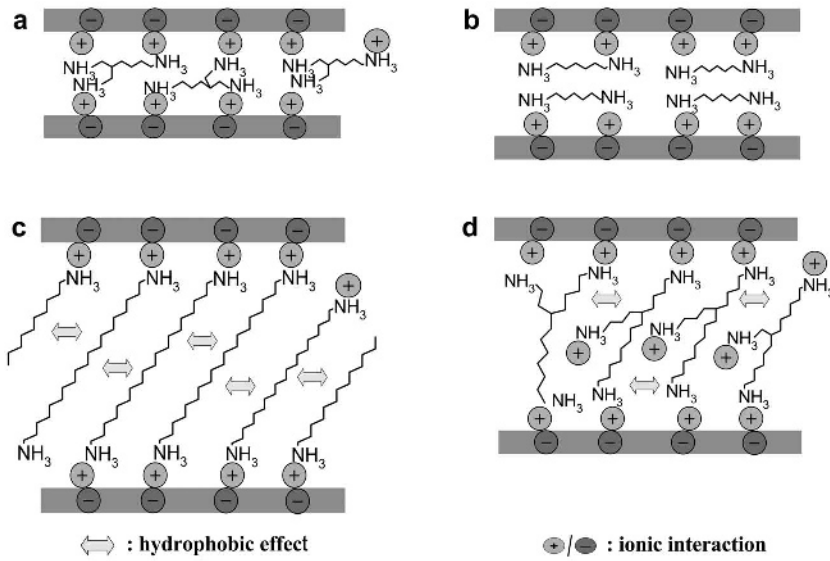

Figure 6. Orientations of POP ammonium ions in the interlayer space of Mt: (a) monolayer, (b) bilayers, and (c,d) inclined arrangements.

spacing (Δd) of T403-Mt (0.61 nm) is similar to the theoretical thickness of the T403 ion chain (at least 0.43 nm). In contrast, the basal spacing of Mt modified with each long-chain ammonium ion (D2000, D4000, T3000, and T5000) was much shorter than the corresponding theoretical length, and the incremental basal spacing (Δd) was much longer than the thickness of the corresponding POP ammonium ion chain (Table 2), implying that these long-chain ammonium ions arranged in an inclined orientation in the interlayers with a certain tilt (Figure 6c,d). The linear relationship between the basal spacing and the theoretical length (Figure 7) can also demonstrate that long-chain ammonium ions were oriented at a certain inclination within the interlayer space.

Effect of chain length on the amount intercalated

To identify the effect of chain length on the amount intercalated and on the thermal stability of the POP ammonium ions intercalated into Mt, the decomposition behaviors of Na^+-Mt and modified Mt were investigated using TGA (Figure 8) and DTG (Figure 9). For both Na^+-Mt and modified Mt, the initial mass loss below 125ºC (Figure 8) was dominated by water. The DTG curve of Na^+-Mt (Figure 9) showed two DTG peaks at 30 and 88ºC, which can be inferred to be due to the mass loss of weakly physisorbed water and of water within the interlayer, and of strongly bonded water of hydration (Na^+), respectively (Xie *et al.*, 2001). However, as for modified Mt, the second peak relating to the mass loss of water absorbed to Na^+ was scarcely observed because

Table 2. Basal spacing (d_{001}) and incremental basal spacing (Δd) of modified Mt as well as the degree of polymerization and theoretical length of the POP amine backbone.

Sample	Basal spacing d_{001} (nm)	Incremental basal spacing Δd[a] (nm)	Intercalating agent[b]	Degree of polymerization	Theoretical length[b] (nm)
Na-Mt	1.25	0.32	–	–	–
D400-Mt	1.76	0.83	D400	6.1	1.4
D2000-Mt	5.50	4.57	D2000	33	7.7
D4000-Mt	8.53	7.7	D4000	68	15.9
T403-Mt	1.54	0.61	T403	6	<1.4
T3000-Mt	5.38	4.45	T3000	50	>7.7
T5000-Mt	7.15	6.22	T5000	85	>13.1

[a] $\Delta d = d_{(\text{modified Mt})} - d_{(\text{layer unit})}$, where $d_{(\text{layer unit})}$, the layer-unit basal distance, is 0.93 nm (Bergaya *et al.*, 2006; Salahuddin, 2004).
[b] Theoretical length was calculated on the basis of the bond lengths (0.154 nm for C–C and 0.143 nm for C–O) and the bond angles (109.6º for C–C and 112º for C–O) (Lin *et al.*, 2001).

https://doi.org/10.1346/CCMN.2011.0590508 Published online by Cambridge University Press

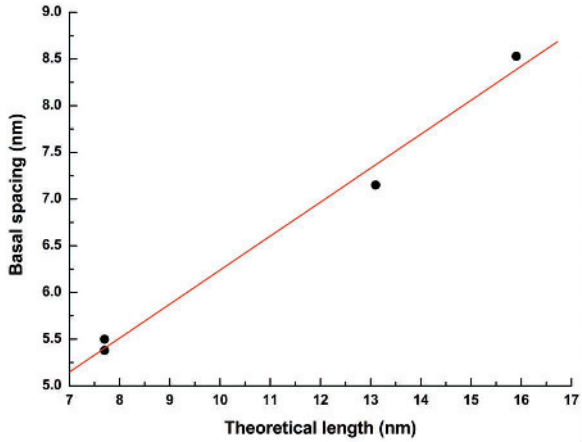

Figure 7. Comparison of the basal spacings of long-chain ammonium ion-modified Mt (D2000-Mt, D4000-Mt, T3000-Mt, and T5000-Mt) and the theoretical lengths of the long-chain ammonium ions.

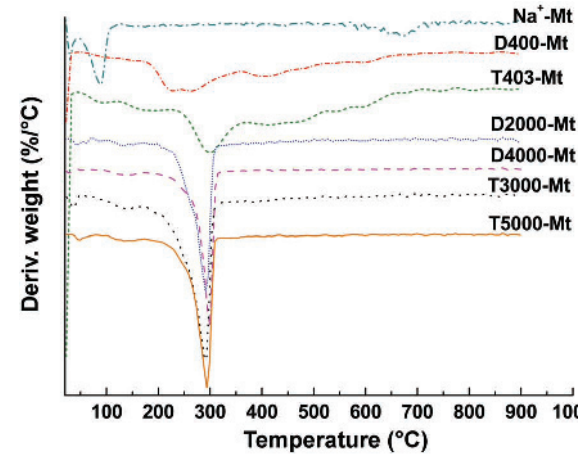

Figure 9. DTG curves of Na^+-Mt and modified Mt.

the Mt became organophilic after intercalation of the POP ammonium ions.

The decomposition behavior of POP amine hydrochlorides was also studied by TG (Figure 10) and DTG (Figure 11), as a reference for analyzing the decomposition behavior of modified Mt. The TG curves (Figure 10) revealed that all POP amine hydrochlorides decomposed in a similar fashion. For the D2000 hydrochloride ion, for example, the main mass loss occurred at temperatures between 278 and 350ºC, and it decomposed almost

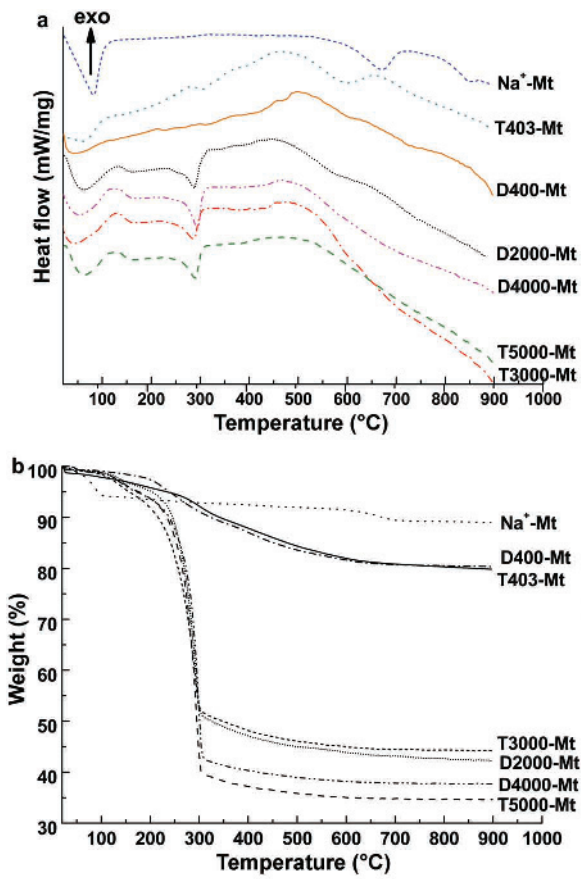

Figure 8. (a) DSC and (b) TGA curves of Na^+-Mt and modified Mt.

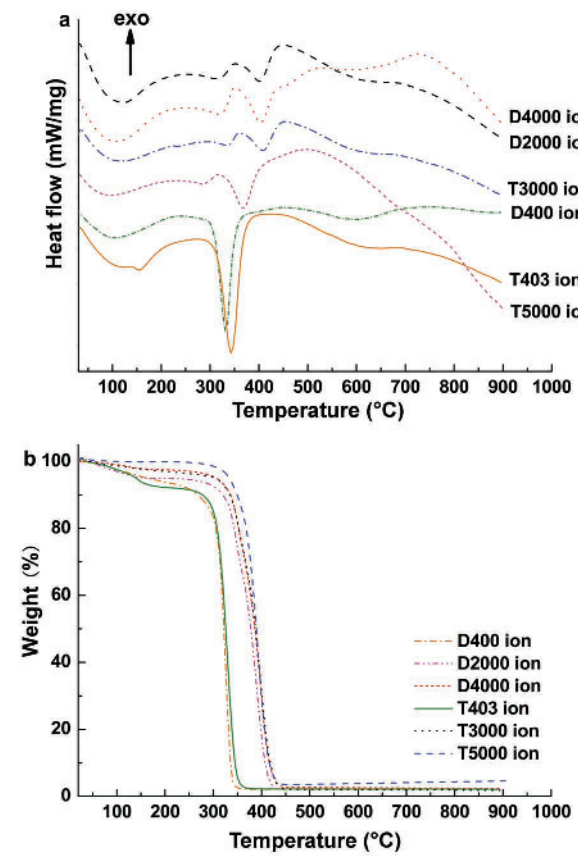

Figure 10. DSC (a) and TGA (b) curves of POP amine hydrochlorides.

https://doi.org/10.1346/CCMN.2011.0590508 Published online by Cambridge University Press

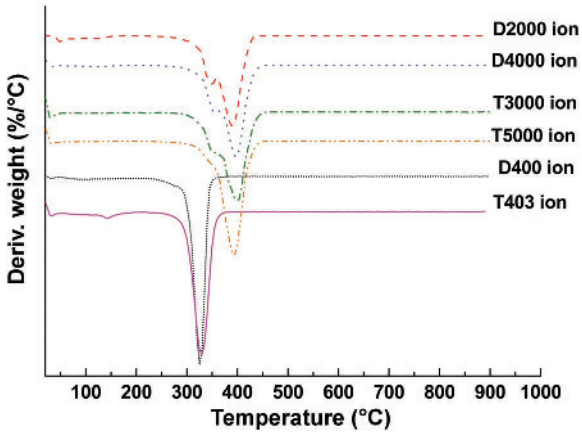

Figure 11. DTG curves of POP amine hydrochlorides.

completely from room temperature to 900ºC. Comparing the TG curves of D2000-Mt and D2000, the mass loss of the D2000 ion in D2000-Mt occurred over a similar temperature range (of 100 [the onset decomposition temperature $T_{onset,1}$] to 350ºC). The total fraction of organic (D2000) ion in modified Mt (wt.%) can be calculated from the mass loss between $T_{onset,1}$ (at 100ºC) and 900ºC of D2000-Mt, corrected with regard to the appropriate mass fraction of Mt in modified Mt for the mass loss associated with Na^+-Mt over the same temperature range, which were mainly composed of the mass losses due to dehydroxylation of the aluminosilicate which occurred between 560 and 750ºC (Figure 8) (Xie *et al.*, 2001; Huskić *et al.*, 2009). The formula for calculating the total organic fraction of modified Mt is illustrated as equation 5.

$$S = [(Y - Z)/1 - Z)] \times 100 \quad (5)$$

where S is the POP ammonium ion fraction in the modified Mt, Y is the mass loss of modified Mt between $T_{onset,1}$ and 900ºC, and Z is the mass loss associated with Na^+-Mt over the same temperature range. On the basis of the total organic fraction (wt.%) and molecular weight of the organic (g/mol), the actual amount of organic in the Mt (mol/g Mt) can be calculated using TGA data *via* the following equation (Xi *et al.*, 2007; Zhou *et al.*, 2009):

$$X = (m \times S \times 10^{-2})/[M \times m \times (100 - S) \times 10^{-2}] = S/[M \times (100 - S)] \quad (6)$$

where X (mol/g Mt) is the amount of POP ammonium ion in the Mt, m is the total weight of the modified Mt, M is the molecular weight of the POP ammonium ion, and S is the POP ammonium ion fraction in the modified Mt. Similarly, the total organic fraction and the actual amount intercalated of the other five POP ammonium ions in the modified Mt can be calculated in the same manner (listed in Table 3). In addition, the theoretical amount intercalated (mol/g Mt) of POP ammonium ions in the Mt was calculated by assuming that Na^+ is fully

Table 3. Decomposition steps for Na-Mt and the modified Mt.

Organoclays	Dehydration	Organic decomposition					Dehydroxylation	Total organic	Theoretical organic	Actual amount of organic in Mt	Theoretical amount of organic in Mt
	T_{max} (ºC)	Mass loss (%) $<T_{onset,1}$	$T_{onset,1}$ (ºC)	$T_{max,1}$ (ºC)	$T_{onset,2}$ (ºC)	$T_{max,2}$ (ºC)	T_{max} (ºC)	(%)	(%)	(mol/g × 10^4)	(mol/g × 10^4)
Na-Mt	30/88.3	3.47	–	–	–	–	670.0	–	–	–	–
D400-Mt	–	1.10	156.3	226.3	245.5	261.3	596.3	14.081	18.100	3.708	5.000
D2000-Mt	40.6	1.28	100.6	135.8	170.6	290.6	–	54.213	50.001	5.914	5.000
D4000-Mt	29.3	1.15	94.3	139.3	174.3	299.3	–	58.974	66.667	3.592	5.000
T403-Mt	–	2.42	116.7	186.7	226.7	296.6	541.7–591.7	13.578	12.613	3.628	3.333
T3000-Mt	36.5	1.52	97.5	142.5	172.5	291.4	–	51.731	50.001	3.569	3.333
T5000-Mt	48.4	1.29	98.4	133.4	173.4	293.4	–	62.194	62.514	3.288	3.333

The percentage of total organic corresponds to the mass loss between $T_{onset,1}$ and 900ºC, corrected with regard to the appropriate mass fraction of Mt in the modified Mt for the mass loss of the same temperature range.

https://doi.org/10.1346/CCMN.2011.0590508 Published online by Cambridge University Press

exchanged by $-NH_3^+$ (listed in Table 3). The actual amount intercalated of each POP triammonium ion was close to that of the corresponding theoretical amount (Table 3), indicating that the ion exchange between inorganic and triammonium ions played a major role in the modification of Mt and occurred almost to completion. Moreover, with increase in chain length of the POP triammonium ions, a slight decrease in the actual amount of POP triammonium ion intercalated in Mt was also observed. A possible explanation was that the steric hindrance of triammonium ions, which was unfavorable to the intercalation of ammonium ions into the Mt interlayers, increased with the chain length of triammonium ions. In contrast, the actual amount of D2000 ion in the modified Mt was greater than its theoretical amount, while the actual amounts of the D400 and D4000 ions were both less than their theoretical counterparts. The reason may be that some of the D400 ions intercalated into D400-Mt were washed out during the triple washing process, due to its much greater solubility in water than that of the D2000 and D4000 ions. For the D4000 ion, the overlong chain length may be unfavorable for intercalation into the interlayer.

Effect of chain length on thermal stability

Six POP ammonium ions in modified Mt all decomposed in a similar fashion to the parent POP ammonium ions. The DTG curves of modified Mt and POP ammonium ions (Figures 9, 11) both showed two DTG peaks associated with the organic decomposition, *i.e.* a major peak preceded by a weak peak; however, the decomposition temperatures (T_{onset} and T_{max}) of POP ammonium ions decreased by various extents after intercalation (Table 4). The decrease in the decomposition temperature of the four long-chain POP ammonium ions (before and after intercalation) became more notable than that of the short-chain D400 and T403 ions (Table 4). Similar phenomena were also observed in the study of Mt modified with quaternary alkyl ammonium (Xie *et al.*, 2001). Generally, the decrease in thermal stability of the intercalating agent was thought to be attributed to the catalytic effect of Lewis or Bronsted acid sites on the aluminosilicate (Xie *et al.*, 2001). The different decreases, on the other hand, were related to the different arrangements adopted by POP ammonium ions in the interlayer space (Figure 6). Short-chain T403 and D400 ions, as mentioned above, lay flat in the interlayer space, thus restricting their thermal motion much more than that of the other four ions which adopted inclined positions in the interlayer space.

In the DTG curves of modified Mt (Figure 9), between 100 and 350ºC, the two DTG peaks, a weak one and a strong one, were both associated with the decomposition of POP ammonium ions. Similar phenomena have been reported for other systems: Xi *et al.* (2004) and Marras *et al.* (2007), who studied thermal stability of Mt modified with octadecyltrimethyl-

Table 4. Change in the thermal stability of POP ammonium ions after intercalation.

Intercalating agent	$T_{onset,1,POP}$ (ºC)	$T_{max,1,POP}$ (ºC)	$T_{onset,2,POP}$ (ºC)	$T_{max,2,POP}$ (ºC)	Modified Mt	$T_{onset,1,clay}$ (ºC)	$T_{max,1,clay}$ (ºC)	$T_{onset,2,clay}$ (ºC)	$T_{max,2,clay}$ (ºC)	$T_{onset,1}$ (ºC)	$T_{max,1}$ (ºC)	$T_{onset,2}$ (ºC)	$T_{max,2}$ (ºC)
D400	215.2	275.2	280.2	326.8	D400-Mt	156.3	226.3	245.5	261.3	58.9	100.5	34.7	65.5
D2000	278	349.4	362.4	400.3	D2000-Mt	100.6	135.8	170.6	290.6	177.4	213.6	191.8	109.7
D4000	281	354.2	360.2	399.2	D4000-Mt	94.3	139.3	174.3	299.3	186.7	214.9	185.9	99.9
T403	–	–	234.1	329.8	T403-Mt	116.7	186.7	226.7	296.6	–	–	7.4	33.2
T3000	278.5	352.3	359.3	402.3	T3000-Mt	97.5	142.5	172.5	291.4	181.0	209.8	186.8	110.9
T5000	280.2	352.1	355.1	394.1	T5000-Mt	98.4	133.4	173.4	293.4	181.8	218.7	181.7	100.7

$T_{onset,1} = T_{onset,1,POP} - T_{onset,1,clay}$, $T_{max,1} = T_{max,1,POP} - T_{max,1,clay}$, $T_{onset,2} = T_{onset,2,POP} - T_{onset,2,clay}$, $T_{max,2} = T_{max,2,POP} - T_{max,2,clay}$. The onset temperature T_{onset} and the temperature at the maximum rate of weight loss, T_{max}, were determined using the DTG curves.

https://doi.org/10.1346/CCMN.2011.0590508 Published online by Cambridge University Press

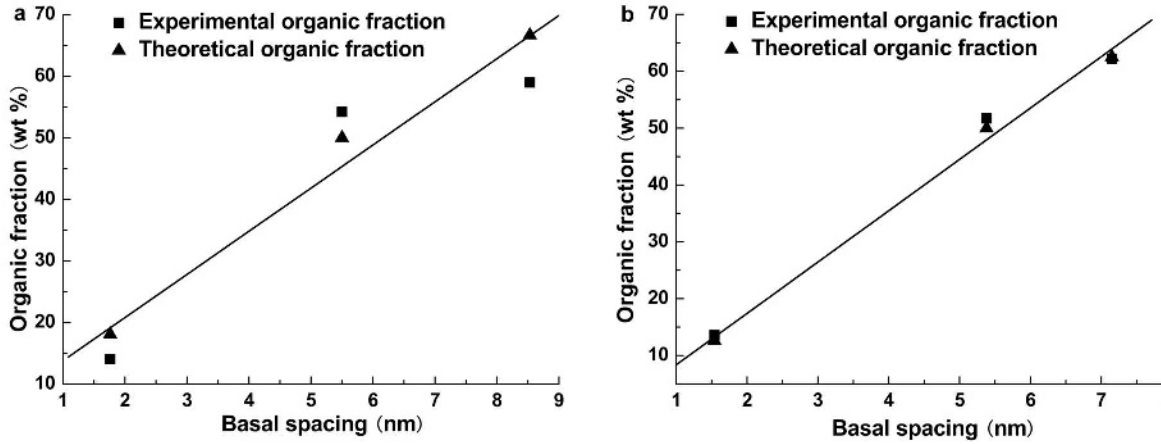

Figure 12. Comparison of the total organic fraction determined by TGA and the theoretical organic fraction calculated by assuming that Na^+ is fully exchanged by $-NH_3^+$ (basal spacing determined by XRD): (a) the Mt modified with POP diammonium ions; and (b) the Mt modified with POP triammonium ions.

ammonium cations and Mt modified with amphiphilic hexadecylammonium cations, respectively, also observed a weak DTG peak accompanying a strong peak. Those authors speculated that the weak peak was attributed to the excess intercalating agent that was attached to the external surface of Mt by van der Waals forces. In order to prove the speculation, the theoretical organic fraction was calculated by assuming that Na^+ is fully exchanged by $-NH_3^+$ (Table 3), and the basal spacing of the modified Mt was compared to the experimental and theoretical organic fractions (Figure 12). The linear correlation (Figure 12) indicated that most of the six POP ammonium ions in the modified Mt were contained within the interlayer space, and, therefore, like the strong DTG peak, the weak DTG peak also resulted from the decomposition of POP ammonium ions within the interlayer space. In addition, the weak DTG peak (Figure 9) may have been derived from the weak DTG peak of parent POP ammonium ions (Figure 11).

CONCLUSIONS

Three POP diamine hydrochlorides and three POP triamine hydrochlorides with different hydrophobic chain lengths were used to modify Mt. The $-CH_2-$ and NH_3^+ vibrations were observed in the FTIR spectra of these modified Mts demonstrating that POP ammonium ions had intercalated into interlayer spaces; after modification, the basal spacings of the Mt were enlarged significantly and increased with the chain length of either POP diammonium ions or POP triammonium ions; the actual amount intercalated (mol/g Mt) of POP triammonium ions was close to the corresponding theoretical amount (mol/g Mt), and decreased slightly with increases in the chain length; compared to the parent POP ammonium ions, the thermal stability of intercalated POP ammonium ions decreased by various extents, *i.e.* a more remarkable decrease in T_{onset} of long-chain POP ammonium ions after intercalation, and a smaller decrease in T_{onset} of short-chain POP ammonium ions. In addition, the linear correlation between the organic fraction and the basal spacing of the modified Mt demonstrated that most of the POP ammonium ions were contained within the interlayer space.

REFERENCES

Alexandre, M. and Dubois, P. (2000) Polymer-layered silicate nanocomposites: preparation, properties and uses of a new class of materials. *Materials Science and Engineering: R: Reports*, **28**, 1–63.

Bergaya, F. and Lagaly, G. (2001) Surface modification of clay minerals. *Applied Clay Science*, **19**, 1–3.

Bergaya, F., Theng, B.K.G., and Lagaly, G., editors (2006) *Handbook of Clay Science*. Elsevier, Amsterdam.

Bergaya, F., Jaber, M., and Lambert, J.F. (2011) *Rubber Clay Nanocomposites Science, Technology and Applications* (M. Galimberti, editor). J. Wiley & Sons.

Becker, O., Varley, R., and Simona, G. (2002) Morphology, thermal relaxations and mechanical properties of layered silicate nanocomposites based upon high-functionality epoxy resins. *Polymer*, **43**, 4365–4373.

Boyd, S.A., Sun, S.B., Lee, J.F., and Mortland, M.M. (1988) Pentachlorophenol sorption by organo-clays. *Clays and Clay Minerals*, **36**, 125–130.

Chen, K.H. and Yang, S.M. (2002) Synthesis of epoxy-montmorillonite nanocomposite. *Journal of Applied Polymer Science*, **86**, 414–421.

Chou, C.C., Shieu, F.S., and Lin, J.J. (2003) Preparation, organophilicity, and self-assembly of poly(oxypropylene)amine-clay hybrids. *Macromolecules*, **36**, 2187–2189.

Esfandiari, A., Nazokdast, H., Rashidi, A., and Yazdanshenas, M.E. (2008) Review of polymer-organoclay nanocomposites. *Journal of Applied Sciences*, **8**, 545–561.

Gu, Z., Song, G.J., Liu, W.S., Yang, S.J., and Gao, J.M. (2010) Structure and properties of hydrogenated nitrile rubber/organo-montmorillonite nanocomposites. *Clays and Clay Minerals*, **58**, 72–78.

Guan, G.H., Li, C.C., and Zhang, D. (2005) Spinning and properties of poly(ethylene terephthalate)/organomontmorillonite nanocomposite fibers. *Journal of Applied Polymer*

https://doi.org/10.1346/CCMN.2011.0590508 Published online by Cambridge University Press

Science, **95**, 1443–1447.

Guegan, R., Gautier, M., Beny, J.M., and Muller, F. (2009) Adsorption of surfactant on a Ca-smectite. *Clays and Clay Minerals*, **57**, 502–509.

Gupta, V.K. and Suhas. (2009) Application of low-cost adsorbents for dye removal – A review. *Journal of Environmental Management*, **90**, 2313–2342.

Hrachová, J., Komadel, P., and Chodák, I. (2009) Natural rubber nanocomposites with organo-modified bentonite. *Clays and Clay Minerals*, **57**, 444–451.

Hsu, R.S., Chang, W.H., and Lin, J.J. (2010) Nanohybrids of magnetic iron-oxide particles in hydrophobic organoclays for oil recovery. *ACS Applied Materials & Interfaces*, **2**, 1349–1354.

Huskić, M., Žagar, E., Žigon, M., Brnardić, I., Macan, J., and Ivanković, M. (2009) Modification of montmorillonite by cationic polyesters. *Applied Clay Science*, **43**, 420–424.

Jaber, M. and Lambert, J.F. (2010) A new nanocomposite: L-dopa/Laponite. *Journal of Physical Chemistry Letters*, **1**, 85–88.

Jaynes, W.F. and Boyd, S.A. (1991) Hydrophobicity of siloxane surfaces in smectites as revealed by aromatic hydrocarbon adsorption from water. *Clays and Clay Minerals*, **39**, 428–436.

Kong, D. and Park, C.E. (2003) Real time exfoliation behavior of clay layers in epoxy-clay nanocomposites. *Chemistry of Materials*, **15**, 19–24.

Lagaly, G. (1981) Characterization of clays by organic compounds. *Clay Minerals*, **16**, 1–21.

Lagaly, G. (1986). Interaction of alkyamines with differents types of layered compounds. *Solid State Ionics*, **22**, 43–51.

Lagaly, G. and Weiss, A. (1969) Determination of the layer charge in mica-type layer silicates. *Proceedings of the International Clay Conference*, Tokyo, **1**, 61–80.

Laza, A.L., Jaber, M., Miehé-Brendlé, J., Demais, H., Le Deit, H., Delmotte, L., and Vidal, L. (2007) Green nanocomposites: synthesis and characterisation. *Journal of Nanoscience and Nanotechnology*, **7**, 1–7.

Lebaron, P.C., Wang, Z., and Pinnavaia, T.J. (1999) Polymer-layered silicate nanocomposites: an overview. *Applied Clay Science*, **15**, 11–29.

Li, Z.H. and Jiang, W.T. (2009) Dodecyltrimethylammonium intercalation into rectorite. *Clays and Clay Minerals*, **57**, 194–204.

Lin, J.J. and Chen, Y.M. (2004) Amphiphilic properties of poly(oxyalkylene)amine-intercalated smectite aluminosilicates. *Langmuir*, **20**, 4261–4264.

Lin, J.J., Cheng, I.J., Wang, R., and Lee, R.J. (2001) Tailoring basal spacings of montmorillonite by poly(oxyalkylene)diamine intercalation. *Macromolecules*, **34**, 8832–8834.

Lin, J.J, Cheng, I.J., and Chen, Y.M. (2003) High compatibility of the poly(oxyalkylene)amine-intercalated montmorillonite for epoxy. *Polymer Journal*, **35**, 411–416.

Lin, J.J., Chou, C.C., Chang, Y.C., and Chiang, M.L. (2004) Conformational change of tri-functional poly(oxypropylene)-amine intercalated in layered silicate confinement. *Macromolecules*, **37**, 473–477.

Lin, J.J., Chen, Y.M., and Yu, M.H. (2007) Hydrogen-bond driven intercalation of synthetic fluorinated mica by poly(oxypropylene)-amidoamine salts. *Colloids and Surfaces A: Physicochem*, **302**, 162–167.

Lin J.J., Chen, Y.M., Tsai, Y.M., and Chiu, C.W. (2008) Self-assembly of lamellar clay to hierarchical microarrays. *The Journal of Physical Chemistry C*, **112**, 9637–9643.

Marras, S.I., Tsimpliaraki, A., Zuburtikudis, I., and Panayiotou, C. (2007) Thermal and colloidal behavior of amine-treated clays: The role of amphiphilic organic cation concentration. *Journal of Colloid and Interface Science*, **315**, 520–527.

Monvisade, P. and Siriphannon, P. (2009) Chitosan intercalated montmorillonte: Preparation, characterization and cationic dye adsorption. *Applied Clay Science*, **42**, 427–431.

Mortland, M.M., Sun, S.B., and Boyd, S.A. (1986) Clay-organic complexes as adsorbents for phenol and chlorophenols. *Clays and Clay Minerals*, **34**, 581–585.

Paiva, L.B. de, Morales, A.R., and Valenzuela Díaz, F.R. (2008) Organo-clays: properties, preparation and applications. *Applied Clay Science*, **42**, 8–24.

Pinnavaia, T.J. and Beall, G.W. (2000) *Polymer-Clay Nanocomposites*, Wiley, Chichester, UK.

Salahuddin, N.A. (2004) Layered silicate/epoxy nanocomposites: synthesis, characterization and properties. *Polymers for Advanced Technologies*, **15**, 251–259.

Salahuddin, N.A., Abo-El-Enein, S.A., Selim, A., and Salah El-Dien, O. (2010) Synthesis and characterization of polyurethane/organo-montmorillonite nanocomposites. *Applied Clay Science*, **47**, 242–248.

Šucha, V., Czímerová, A., and Bujdák, J. (2009) Properties of I-S minerals from Rhodamine 6G dye interactions. *Clays and Clay Minerals*, **57**, 361–370.

Wang, S.Z. and Zang, X.S. (1991) *Modern Research Methods of Materials*. Beihang University Press, China (in Chinese).

Xi, Y.F., Ding, Z., He, H., and Frost, R.L. (2004) Structure of organo-clays – an X-ray diffraction and thermogravimetric analysis study. *Journal of Colloid and Interface Science*, **277**, 116–120.

Xi, Y.F., Frost, R.L., He, H.P., Kloprogge, T., and Bostrom, T. (2005) Modification of Wyoming montmorillonite surfaces using a cationic surfactant. *Langmuir*, **21**, 8675–8680.

Xi, Y.F., Frost, R.L., and He, H.P. (2007) Modification of the surfaces of Wyoming montmorillonite by the cationic surfactants alkyl trimethyl, dialkyl dimethyl, and trialkyl methyl ammonium bromides. *Journal of Colloid and Interface Science*, **305**, 150–158.

Xie, W., Gao, Z.M., Pan, W.P., Hunter, D., Singh, A., and Vaia, R. (2001) Thermal degradation chemistry of alkyl quaternary ammonium montmorillonite. *Chemistry of Materials*, **13**, 2979–2990.

Yadav, L.D.S. and Rai, V.K. (2006) Chemoselective annulation of 1,3-dithiin, -thiazine and -oxathiin rings on thiazoles using a green protocol. *Tetrahedron*, **62**, 8029–8034.

Yoon, K.B., Sung, H.D., Hwang, Y.Y., Noh, S.K., and Lee, D.H. (2007) Modification of montmorillonite with oligomeric amine derivatives for polymer nanocomposite preparation. *Journal of Applied Polymer Science*, **38**, 1–8.

Zhao, Q. and Samulski, E.T. (2006) A comparative study of poly(methyl methacrylate) and polystyrene/clay nanocomposites prepared in supercritical carbon dioxide. *Polymer*, **47**, 663–671.

Zhou, L.M., Chen, H., Jiang, X.H., Lu, F., Zhou, Y.F., Yin, W.M., and Ji, X.Y. (2009) Modification of montmorillonite surfaces using a novel class of cationic gemini surfactants. *Journal of Colloid and Interface Science*, **332**, 16–21.

(*Received 8 August 2010; revised 11 November 2011; Ms. 467; A.E. H. Dong*)

https://doi.org/10.1346/CCMN.2011.0590508 Published online by Cambridge University Press